Foamed gypsum for multipurpose applications in building

Ilaria Capasso [a], Lucia Pappalardo [b], Rosario Aniello Romano [c], Fabio Iucolano [d*]

[a] *Department of Engineering and Geology, University of Chieti-Pescara "G. d'Annunzio", Viale Pindaro 42, Pescara 65127, Italy*

[b] *Istituto Nazionale di Geofisica e Vulcanologia, sezione di Napoli-Osservatorio Vesuviano, via Diocleziano 328, Naples 80124, Italy*

[c] *Department of Industrial Engineering, University of Naples Federico II, P.le Tecchio 80, Naples 80125, Italy*

[d] *ACLabs - Applied Chemistry Labs, Department of Chemical, Materials and Industrial Production Engineering, University of Naples Federico II, P.le Tecchio 80, Naples 80125, Italy*

* *Corresponding author, email: fabio.iucolano@unina.it*

Abstract

Gypsum plasterboards are nowadays very appreciated in buildings, mainly due to their lightness, thermal insulation and suitable sound transmission loss when used in double walls. However thermal and acoustic features of gypsum plasterboard can be enhanced. In the present study an innovative method, consisting in the direct addition of a pre-manufactured foam to gypsum pastes is used to increase the gypsum porosity improving sound absorption, lightness and thermal insulation features. In this aim, the role of both different amounts and dilutions of a vegetal foaming agent on the main physical, mechanical and microstructural characteristics of the gypsum was experimentally investigated. Moreover, also X-ray computed micro tomography technique (Micro-CT) was carried out in order to investigate the 3D internal microstructure of the materials. The results confirmed the effectiveness of the foaming agent in increasing the gypsum porosity, with a linear correlation between densities and mechanical strengths. Moreover, the presence of large bubbles, mainly connected each other, involved in a strong reduction of the thermal coefficient (λ), from 0.57 W/m·K of REF sample to 0.25 W/m·K of LG10_5% sample, and in a strong increase of the normal sound absorption coefficient (α_0), from 0.06 of REF sample to 0.20 of LG10_5% sample. Finally, in

the light of the results obtained by the present research, the use of a pre-whipped vegetal foaming agent represents a suitable way to obtain lightweight gypsum-based materials with enhanced thermal and acoustic properties.

Keywords: lightweight gypsum; foaming agent; thermal insulation; acoustic absorption, micro-tomography.

1. Introduction

Gypsum can be considered as one of the most eco-sustainable building materials and so, in recent years, its relevance in construction industry is considerably growing. In fact, thanks to the lower calcination temperature, especially if compared with cement and/or lime, gypsum manufacturing requires reduced energy consumption. Moreover, several waste products, such as phospho-gypsum [1] and flue gas desulfurization (FGD) gypsum [2], can be used in gypsum manufacturing, promoting the reuse of secondary raw materials. In addition to being an environmentally friendly material, gypsum exhibits many advantages, such as excellent fire-protecting and heat-resistant properties, good workability and fast setting, aesthetic appearance, acoustic insulation and humidity controlling abilities [3–6]. Despite these numerous advantages, the most common utilization of gypsum in buildings is mainly limited to the production of gypsum boards, flooring and ceiling panels, interior plasters [3,7]. In order to promote new possible applications for gypsum based materials, it is possible to improve some specific gypsum properties, such as mechanical strengths [8,9], lightness, thermal insulation features and sound absorbing properties [10–12] with respect to traditional gypsum plasters. This need is particularly required for historical buildings restoration, above all for those protected by the Superintendence of Cultural Heritage, where the use of higher performing materials is often prohibited. The most common way to enhance the thermal insulation and sound-absorbing properties of gypsum matrices and of materials in general, is to act on their porosity, allowing at the same time also to improve their performance in terms of strength to weight ratio, which represents a key parameter especially for building materials. In fact, porous materials show a wide number of peculiarities which make them suitable for numerous and multipurpose applications, according to the features of their porosity such as pores amount, distribution, shape, size, connectivity, etc. [13]. Among the several applications of porous materials (heavy metal absorption, catalysis, energy storage, filtration membranes, etc.), the ones concerning with thermal insulation and sound-absorbing behavior are the most interesting for building materials. Currently,

the most common materials used for this purpose are polymers, especially polyurethane and polystyrene, but, they are highly flammable [14]. So, the main interests of research activity is now focused on the development of inorganic, fire-resistant thermal insulation materials [7][15]. A great attractive is nowadays represented by foamed glasses, a promising alternative material for the thermal and acoustic insulation of buildings, which exhibit several interesting features, such as high insulation capacity, a very long lifespan, recyclability and non-flammability [16]. In this context, also gypsum foams result to be a valuable material to be used for multipurpose applications in buildings, with a favorable compromise between mechanical, thermal and acoustic features, sustainability, cheapness, and no toxicity [17][11][18]. Several innovative strategies have been recently explored to increase and tailor properly the porosity of materials [14,19,20] and referring to the gypsum, the most widely used techniques consist in the addition of chemical additives, lightweight aggregates or air-voids [5,6,21,22]. In particular, chemical additives allow to embed pores into the gypsum matrices by two mechanisms, gas-producing chemical reaction [7,23] and mechanical foaming by means of surface active substances. The effect of surface active substances, or surfactants, is the lowering of the surface tension. This effect can be achieved by strongly whisking at high speed the gypsum mixture, after adding surfactants directly into the slurry, or cautiously mixing pre-whipped foams, consisting of water and chemical surfactants, into the gypsum paste [3,12,21,24]. The addition of pre-manufactured foams to inorganic mixtures, widely known as physical foaming, is typical of the production of porous ceramic materials, and allows to obtain a more stable and fine pored product as final result of foaming process [25]. Moreover, selecting suitably the whipping conditions of pre-manufactured foams, especially whipping rate, it is possible to obtain stable foam networks, able to act as ‘‘meringue’’ type foams, maintaining themselves during the hardening processes of the inorganic matrix [26].

In the present paper, gypsum matrices have been lightened by means of physical foaming, using a pre-manufactured foam obtained from a water solution, containing natural surfactants. The use of a physical foaming to produce lightened gypsum matrices represents an innovative technique which is up to now scarcely investigated in scientific literature. Moreover, the role of different amounts and concentrations of the foaming agent solution on the final features of the lightweight gypsum have been widely investigated. Finally, a deep characterization of the 3D microstructure has been carried out, in order to assess the correlation between the porosity morphology and the physical, mechanical, morphological, thermal insulating and sound-absorbing properties of so obtained gypsum composites.

2. Experimental

2.1 Materials

Gypsum used in the manufacturing of lightweight samples was a commercial product by Gyproc Saint-Gobain (Milano, Italy) and its main constituent is calcium sulphate hemihydrate ($CaSO_4 \cdot 0.5H_2O$). The chemical composition of gypsum was evaluated by simultaneous thermal analysis (DSC-TGA) (temperature range: 20-1000 °C; heating rate: 10 °C/min; atmosphere: N_2), using a Netzsch STA409PC Luxx apparatus. The mineralogical composition of the binder was evaluated by XRD analysis on powdered samples using a Panalytical X'Pert Pro diffractometer, equipped with PixCel 1D detector (operative conditions: CuKα1/Kα2 radiation, 40 kV, 40 mA, 2Q range from 5 to 80°, step size 0.0131° 2Φ, counting time 40 s per step). In order to complete the chemical characterization of the raw gypsum, FT-IR analyses were carried out at room temperature by using a PerkinElmer Spectrum 3 Tri-Range FT-IR spectrometer apparatus and selecting a wavenumber resolution of 4 cm^{-1} for 32 scans from 4000 to 550 cm^{-1}. The FT-IR spectra were collected in ATR absorbance mode.

The foaming agent (FA) was supplied by Isolchem s.r.l. Italia (commercial name ISOCEM S/L) and it is a liquid solution made of water, vegetal proteins and natural surfactants, mainly fatty acids. The foaming agent was further diluted, in bi-distilled water, before being added to water-gypsum paste. In particular, two dilutions ($wt_{FA}/wt_{FA+water}$) had been selected, which were respectively 5% and 10%.

2.2 Preparation of lightweight gypsum samples

2.2.1 Foaming agent properties and whipping process

ISOCEM S/L has already been used, not diluted, as foaming agent for gypsum composites in a previous paper [12]. In the present paper, the two diluted foaming agent solutions were whipped for 60 s, at about 12000 rpm, with a Moulinex HM6151 Powermix mixer, before being added to the gypsum paste. In order to investigate the foaming behavior of the two ISOCEM S/L dilutions and the stability of the produced foams, the two solutions diluted at 5% and 10% were first whipped in 600-mL glass beakers for 60 s and then the obtained foams were held for 30 min. Foaming properties have been evaluated by means of three parameters: relative overrun (RO), foam stability (FS), and liquid drainage (LD) [27,28]. In particular, RO allowed to define the foaming capacity and it was calculated as reported in Fig.1 (see Eq. (1)), while FS and LD were calculated using respectively Eq.(2) and Eq.(3) (see Fig.1) [28,29]. The same parameters were also evaluated for the

pure foaming agent in order to verify the potential effect of the dilution on foaming capacity and/or stability. Three measurements were carried out for each mixture.

$$RO = \frac{V_0}{V_i} \quad (1)$$

$$FS = \frac{V_{30}}{V_0} \quad (2)$$

$$LD = 1 - \frac{(V_i - V_{L30})}{(V_i - V_{L0})} \quad (3)$$

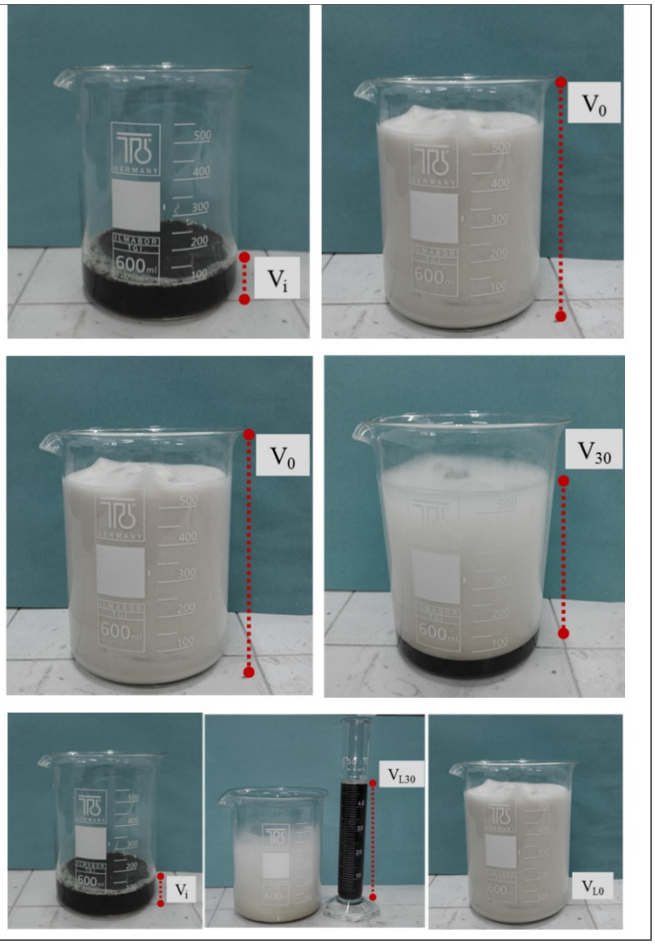

Figure 1 Evaluation of foaming properties and calculation of relative overrun (RO), foam stability (FS), and liquid drainage (LD). V_i = volume of initial liquid, V_0 = volume of foam after 1min whipping, V_{30} = volume of foam at 30 min, V_{L30} = volume of liquid at 30 min, V_{L0} = volume of liquid after 1min whipping.

2.2.2 Preparation and characterization of gypsum pastes

Gypsum pastes were prepared at room temperature adding the previously dry homogenized gypsum powder to the bi-distilled water and mixing for about 60 s with a paddle stirrer. A fixed water to gypsum ratio (wt/wt), equal to 0.6, was selected. Then, different amounts of the foaming agent solution, diluted and whipped as previously described, were added to the paste and the resulting mixtures were mixed for further 60 s. The quantities of whipped foaming agent added were calculated as weight percentage in respect to the gypsum, so 5 wt%, 7.5 wt% and 10 wt% were selected. Preliminary investigations demonstrated that a lower amount of whipped foam led to no

significant lightening of the specimens, whereas a higher amount led to lighter specimens with scarce mechanical features. Furthermore, gypsum plasters (water to gypsum ratio still 0.6) without adding foaming agents to the water-gypsum paste, were produced as reference material. All the produced mixtures were first poured in open molds of several geometries and compacted using a vibration table and then, after that setting time had reached, the hardened specimens were demolded and cured at 40°C for 48 h. After curing, specimens were placed in a climatic cell (T=20°C, H_R=50%) to ensure that homogeneous conditions of temperature and relative humidity were reached before performing the experimental tests. The compositions and the labels of the reference (REF) and of the lightweight gypsum samples (LG) are summarized in Table 1.

Table 1. Lightweight gypsum mixtures compositions and labels.

Sample	w/g ratio	Foaming agent amount (wt. %)	Foaming agent dilution (wt. %)
REF	0.6	/	/
LG5_5%	0.6	5	5
LG7.5_5%	0.6	7.5	5
LG10_5%	0.6	10	5
LG5_10%	0.6	5	10
LG7.5_10%	0.6	7.5	10
LG10_10%	0.6	10	10

The setting times of REF and LG samples were evaluated according to the Vicat test [30], as the increase of porosity in lightweight gypsum samples could affect their setting behavior [18]. All the measurements, both for initial and final setting times, were carried out in triplicate.

2.3 Characterization of hardened lightweight gypsum samples

2.3.1 Physical characterization

The open porosity and the water absorption were evaluated according to UNI 11060 [31] on cubic specimens (5 cm side), so the experimental test allowed to know the amount of water uptake (wt%) after full immersion. The samples were first dried at 60±5°C until constant mass was reached (M_1, g) and then immersed in water in an evacuation vessel at room temperature under vacuum. Vacuum condition was maintained constant for 2 h, pressure was then returned to atmospheric condition and

the samples were weighed immersed in water (hydrostatic weighing, M_2, g). Finally, after being softly wiped with a damp cloth, samples were weighed again, determining the mass of the water-saturated samples (M_3, g). The water absorption is calculated as follows:

$$\frac{M_3 - M_1}{M_1} \times 100 \quad (4)$$

Then, nondestructive measurements of ultrasonic P-wave velocity (UPV) were performed according to UNI EN 14579 [32] by means of a BOVIAR DSP UTD 1004 Ultrasonic device (55 kHz transducers in direct arrangement) in order to qualitatively estimate the porosity change between reference and lightweight gypsum samples. In fact, ultrasonic techniques are widely used to investigate the presence of cracks or defects in materials [33] and then to analyze the materials microstructure development [34]. Moreover, if UPV is used in association with tomography, it can provide even more satisfying qualitative information about the variations occurring in materials properties as well as on their microcracking state [35]. All the experimental test above described were carried out in triplicate.

2.3.2 Mechanical characterization

Flexural and compressive tests were performed on both REF and LG samples using a Tensometer 2020 apparatus and according to UNI EN 1015-11 [36]. In particular, the flexural tests were carried out on prismatic samples (40 x 40 x160 mm) with a load cell of 500 N and a crosshead rate of 1 mm/min. Compression strength tests were carried out on the cubic (40 x 40 x 40 mm) fragments, resulting from the flexural tests, with a load cell equal to 10 kN and a crosshead rate equal to 2 mm/min. All the measurements were performed in triplicate.

2.3.3 X-ray Micro-tomography characterization

X-ray computed microtomography (Micro-CT) is a powerful technique for visualization, inspection and quantitative investigation of the 3D internal microstructure of materials. Micro-CT allows to explore samples in three dimensions, non-destructively and at high resolutions (down to the submicron), through the reconstruction of three-dimensional digital maps (in function of differences in density and atomic number in the scanned sample). From these digital maps, key quantitative information can be directly extracted in 3D (e.g., 3D distribution of content, size, shape, orientation of pores, fractures, minerals, grains, etc).

In this study, microtomographic analyses have been performed using a Carl Zeiss Xradia Versa-410 3D X-ray microscope. This system includes a polychromatic microfocus X-ray source (40-150kV, maximum 10W) that allows the scanning of samples with a wide range of density and a 2k x 2k pixel, noise suppressed charge-coupled detector equipped with different magnification objectives (0.4x, 4x, 10x, 20x) that allow a high resolution, up to 0.9 micron/voxel. Samples of diameter 0.5 cm were scanned in absorption mode, acquiring 4001 projections over a 360° rotation at 90-80 KV and 8-7 W with objective 4x. The resulting nominal voxel (volumetric pixel) size is 5.08 μm. Moreover for the reference gypsum sample (REF) a higher resolution scan with a nominal voxel of 2 μm (objective 10x) has also been acquired in order to detect and measure the smaller (< 5-10 μm) pores population inside the matrix. For LG samples the percentage of matrix pores has been estimated considering the content of matrix pores in REF as reference value.
The tomographic reconstruction was achieved through a filtered back-projection algorithm using XRM Reconstructor software, thus producing a stack of 967 cross-sectional, grey-scale digital images. Image analyses were performed by using the Dragonfly (ORS) and Avizo (FEI) program and following the procedure described by Pappalardo et al.[37] and Liedl et al. [38].

2.3.4 Characterization of thermal insulation and sound-absorbing behavior

Thermal insulation

In order to investigate the thermal insulating properties of both REF and LG samples, the thermal conductivity was measured according to ASTMWK50791-WK43689 [39][40]. Experimental tests were performed at ambient conditions on cylindrical slabs (d = 10 cm, h = 2 cm) using a thermal conductivity analyzer (C-Therm Technologies, Fig.2) whose operating principle is the Modified Transient Plane Source (MPTS) method. For each sample typology, five tests were performed.

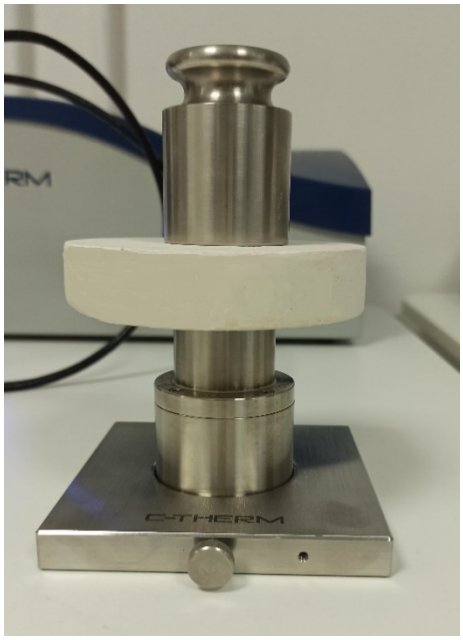

Figure 2 Apparatus for thermal conductivity measurement.

Acoustic absorption

The normal incidence sound absorption coefficient α_0 of both REF and LG samples was measured by means of the transfer function method proposed by Chung and Blaser [41] and reported in the ISO 10534-2 Standard [42]. In particular the SCS9020B Impedance Tube provided by VIBRO-ACOUSTIC srl was used. The measurements were performed placing the rigid backed specimens being tested at an end of a 10 cm diameter standing wave tube, while at the other end of the standing wave tube was mounted a loudspeaker fed by a white noise signal. Each tested sample was cut into circular slices with flat faces and, to avoid any air leakage along the lateral edges of the specimen in contact with the internal surface of the tube attached to the tube, the edges of the specimen were sealed using vaseline grease. The sound pressure was picked up at two locations along the wall of the tube, spaced 50 mm each other. Given the standing wave tube diameter and the distance between the positions of the microphones, the measurements were carried out in the frequency range between 350 Hz and 1750 Hz. A sketch of the measurement set-up is shown in Fig. 3.

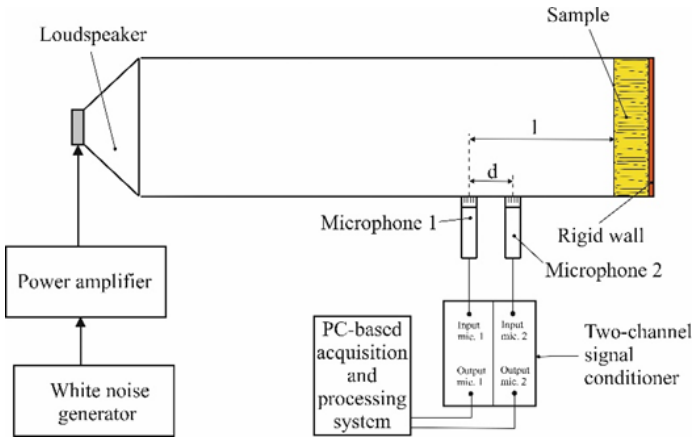

Figure 3 Apparatus for normal incidence sound absorption coefficient measurement.

The measurement of the sound pressure signals at the two positions allows to calculate the transfer function $H_{12}(f)$ between the two microphones as follows:

$$H_{12}(f) = \frac{FFT(p_2)}{FFT(p_1)} \quad (5)$$

where p_1 and p_2 are, respectively, the sound pressure impulse response at the microphone position nearest to the loudspeaker and the tested sample. From the knowledge of the transfer function $H_{12}(f)$, the complex reflection coefficient at the surface of the specimen, taking into account for the plane sound wave assumption, is given by:

$$R(f) = \frac{H_{12} - e^{-jk_0 d}}{e^{jk_0 d} - H_{12}} e^{jk_0 l} \quad (6)$$

In Eq. 6 k_0 is the wavenumber whereas l and d, as shown in Fig. 3, are respectively the distance of microphone 1 from the tested samples and the distance between two measurement microphones.

Then the normal incidence sound absorption coefficient α_0 is obtained by:

$$\alpha_0 = 1 - |R(f)|^2 \quad (7)$$

The measurements were performed on three LG samples, one for each percentage of considered FA, and on a sample of reference gypsum. For each sample the measurements were repeated three times and the results were averaged. To take into account for low sound attenuation of the measurement equipment, the measurements were carried out on a rigid wall as well and for automatic calibration of amplitude and phase for two measurement microphones, the microphone switching technique proposed by Chung and Blaser [43] was used.

3. Results and discussion

3.1 Characterization of raw materials

In Fig. 4 the thermal (a) and XRD (b) analysis of raw gypsum were reported. The thermal analysis revealed the presence of two main peaks. The first, around T=140°C, is representative of the de-hydration of hemihydrate (see Eq. (8)):

$$CaSO_4 \cdot ½H_2O \rightarrow CaSO_4 + ½H_2O \quad (8)$$

This reaction indicates that the de-hydration of 1 mol of $CaSO_4 \cdot ½H_2O$ (145 g) generates a weight loss corresponding to 0.5 mol of H_2O (9 g), which represent a weight loss of 6.2%. Therefore, as the measured weight loss referred to the first peak is equal about to 5.5%, the amount of hemihydrate (H) in the raw gypsum is about 89%. A second peak was detected around T=740°C, and was relative to the decomposition of calcite (see Eq. (9)):

$$CaCO_3 \rightarrow CaO + CO_2 \quad (9)$$

This reaction indicates that the calcination of 1 mol of $CaCO_3$ (100g) produces a weight loss corresponding to 1 mol of CO_2 (44 g), which represent a weight loss of 44%. Therefore, as the measured weight loss referred to the second peak is equal about to 4%, the amount of calcite (C) in the starting raw gypsum is about 9%. Finally, the remaining part of the raw gypsum (about 2-3%) mainly consists of anhydrite, whose presence, together with the above-mentioned hemihydrate (H) and calcite (C), was confirmed by XRD analysis (Fig. 4b). The presence of carbonate species was further confirmed by ATR-FTIR results reported in Fig. 4c. In particular, the spectrum of the raw gypsum showed two peaks characteristic of the presence of carbonate anions: one band centered around 1453 cm^{-1}, typical of the C─O stretching mode and a narrow band at 873 cm^{-1} related to the bending mode [44]. Moreover, the IR spectrum showed the presence of typical vibration bands of gypsum, centered at around 1113, 660, and 600 cm^{-1} as well as the stretching and deformation vibrations of the O–H bond of water at 3580, cm^{-1} and at around 1627 cm^{-1}, respectively [44,45].

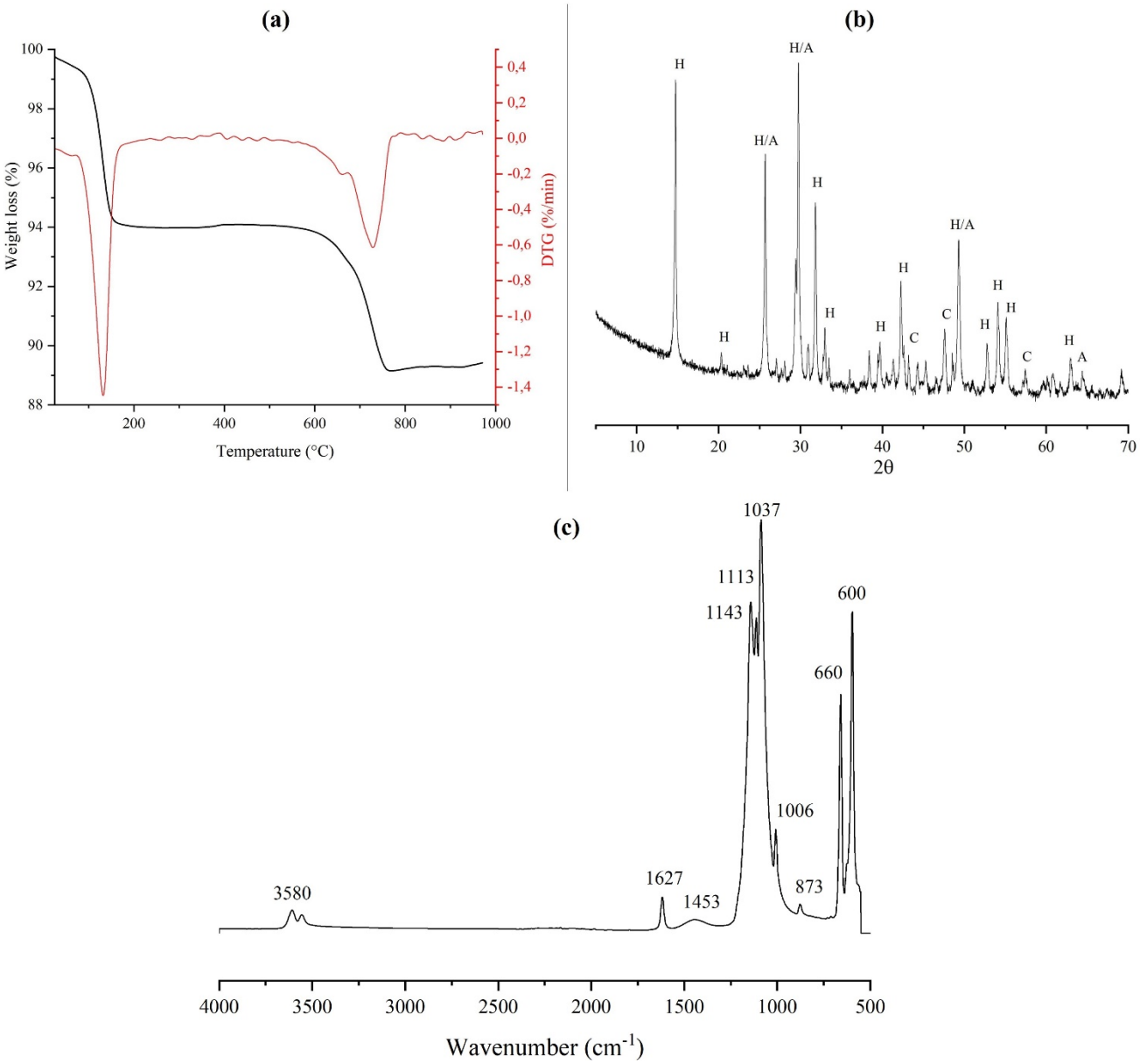

Figure 4 Characterization of gypsum powder: (a) thermogravimetric analysis (black line) and its first derivative (red line); (b) XRD spectrum. H = Hemihydrate; A = Anhydrite; C = Calcite; (c) FT-IR spectrum of gypsum powder.

The main properties of the FA, evaluated as widely described in section 2.2.1, are reported in Table 2. By inspecting the table, it is possible to assess that the foam stability is definitely not affected by the dilution process, in fact its value is basically the same for pure foaming agent and for both dilutions. The foaming capacity, instead, slightly decreases when the foaming agent concentration lowers, in fact the RO value results to be reduced of about 8% passing from the pure foaming agent

to the 5% dilution. Moreover, the use of diluted foaming agent solutions leads to a moderate increase of liquid drainage, regardless of the foaming agent amount.

Table 2 Foaming agent properties of pure and diluted foaming agent.

	Foaming agent dilution		
	Pure FA	**10%**	**5%**
Relative overrun	6.10 ± 0.10	5.80 ± 0.12	5.60 ± 0.11
Foam stability	0.81 ± 0.05	0.81 ± 0.04	0.78 ± 0.05
Liquid drainage	0.78 ± 0.09	0.90 ± 0.10	0.90 ± 0.08

3.2 Physical characterization of fresh and hardened lightweight gypsum

In Table 3 both the initial and final setting times of all the manufactured samples were reported. The data indicate that the use of surfactant foaming agent leads, on the whole, to faster setting times, because of the surface tension reduction, due to the effect of surfactants addition, and the following increase of the dissolution phenomenon of gypsum hemihydrate [18]. However, this trend appears to be less evident with the increasing of the FA, i.e. for both dilutions no significant variation on setting times occurs passing from 7.5% to 10% of FA amount.

Table 3 Initial and final setting times of the lightweight gypsum samples.

Sample	**Setting time (min)**	
	Initial setting	Final setting
REF	35.0 ± 0.5	38.5± 0.5
LG5_5%	31.0 ± 0.5	34.5 ± 0.5
LG7.5_5%	27.0 ± 1.0	31.0 ± 0.5
LG10_5%	27.5 ± 1.0	30.5 ± 1.0
LG5_10%	32.0 ± 0.5	37.0 ± 0.5
LG7.5_10%	30.5 ± 0.5	35.0 ± 1.0
LG10_10%	30.0 ± 1.0	34.0 ± 1.0

The main physical properties of all the manufactured samples are reported in Table 4 (and compared with reference gypsum). By inspecting these data, the role of the FA on the porosity increase of gypsum matrices is strongly evident. In fact, for both the dilutions (5% and 10%), FA addition led to an increase of the open porosity from ≈47% (REF) up to ≈70% (LG10_5% and LG10_10%). In particular, it is worth noting that most of this increase is already achieved for

foaming agent additions of 7.5% and that a similar behavior can be recorded also for the water absorption and for the apparent density, which decreases following this same trend. Regarding the values of real density, all the samples show basically the same result, as expected taking into consideration that the real density is related only to the gypsum matrix, which is always the same. Finally, the different dilutions of FA do not affect considerably all the above discussed physical properties.

The strong increase of the porosity due to the above discussed addition of FA, also influences the measurements of ultrasonic P-wave velocity (UPV), summarized in Table 5. These data exhibit an evident reduction of UPV with the increasing of FA amount, mainly up to 7.5% addition of FA, while a further addition (from 7.5 to 10% of FA) does not led to a significant UPV reduction. This trend is consistent with the above discussed role of the FA on the LG porosity. Similarly, there is not an evident role played by the FA dilution on the UPV measurements.

Table 4 Main physical properties of reference and lightweight gypsum mixtures (average values ± standard deviations are reported).

Sample	Apparent density (g/cm^3)	Real density (g/cm^3)	Open Porosity (%)	Water absorption (%)
REF	1.20 ± 0.02	2.25 ± 0.04	46.68 ± 0.75	38.91 ± 0.87
LG5_5%	0.86 ± 0.05	2.27 ± 0.06	62.03 ± 0.83	72.60 ± 1.06
LG7.5_5%	0.72 ± 0.03	2.34 ± 0.05	69.11 ± 0.87	89.51 ± 1.20
LG10_5%	0.67 ± 0.09	2.29 ± 0.05	70.85 ± 0.68	89.43 ± 1.35
LG5_10%	0.86 ± 0.06	2.28 ± 0.05	62.00 ± 0.94	72.54 ± 0.98
LG7.5_10%	0.74 ± 0.01	2.32 ± 0.01	67.95 ± 0.72	88.78 ± 1.23
LG10_10%	0.68 ± 0.06	2.30 ± 0.01	70.45 ± 0.88	90.83 ± 1.42

Table 5 Ultrasonic pulse velocity (UPV) for REF and LG samples.

Sample	UPV (m/s)
REF	2150.54 ± 19.31
LG5_5%	1652.89 ± 23.56
LG7.5_5%	1462.52 ± 26.76
LG10_5%	1426.02 ± 38.15

LG5_10%	1639.34 ± 18.56
LG7.5_10%	1483.68 ± 21.36
LG10_10%	1406.96 ± 24.57

3.3 Mechanical characterization

The results of flexural and compressive tests are described by the curves reported respectively in Figs. 5 and 6, while the average values of flexural and compressive strengths are listed in Table 6. As expected, the addition of FA caused a reduction of both flexural and compressive strengths due to the porosity increase [46]. Moreover, regarding the flexural behavior (see Fig. 5), it is worth noting that also the elastic modulus of the lightweight gypsum samples decreased proportionally with the amount of foaming agent added. Finally, in accordance with the results reported in the previous section, the different dilutions of the foaming agent seem to not affect the mechanical performance of LG samples.

Looking at the curves depicted in Figure 6, a toughening effect can be noted for all the LG samples. This effect, totally absent for the reference sample, which showed the typical brittle behavior, can be related to the gradual collapse of the porosity. The foamed samples, showed an initial linear elastic behavior and then, after that the maximum load has been reached, small load falls can be detected and probably due to the pore strut fractures [47]. Then, the following small load increases can be explained as a consequence of the densification process due to the collapse of pore structure. In fact the porosity acts firstly as a microcracks, causing load falls and then as densifier agent, causing the load increases. This behaviour led the porous gypsum matrices to support further loads without brittle cracking [12,47]. The above mentioned “densification process” is macroscopically evident looking at the surface of the LG samples after the compressive test. As an example, the surface of the sample LG10_5% is reported in Fig. 7. Finally, Fig. 8 demonstrates that the compressive strengths are linearly correlated to the density, with a satisfactory correlation coefficient (R^2).

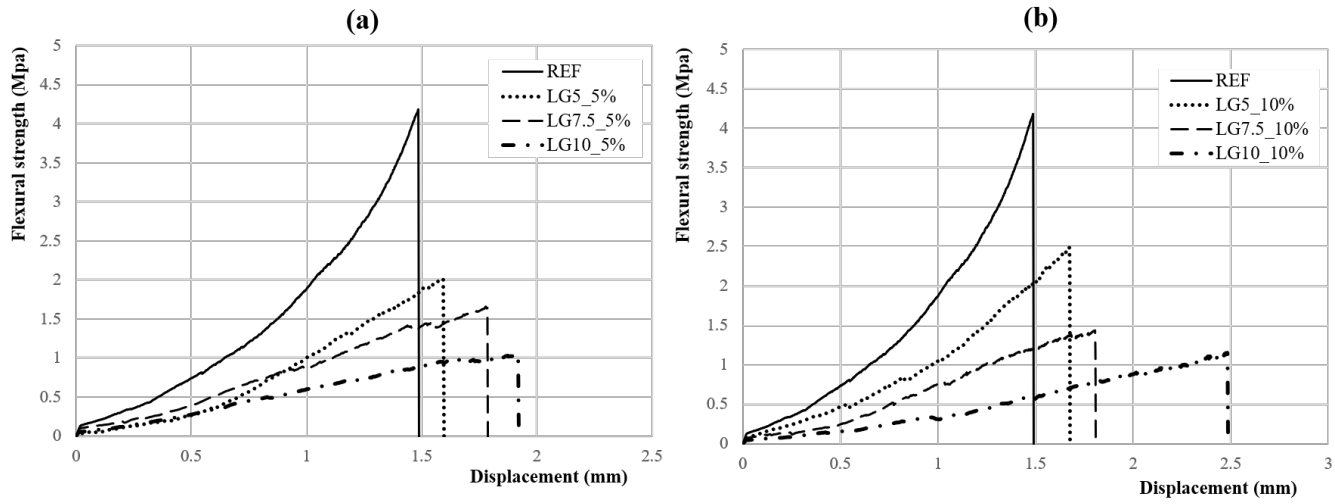

Figure 5 Flexural strengths of LG produced with foaming agent diluted respectively at 5% (a) and 10% (b).

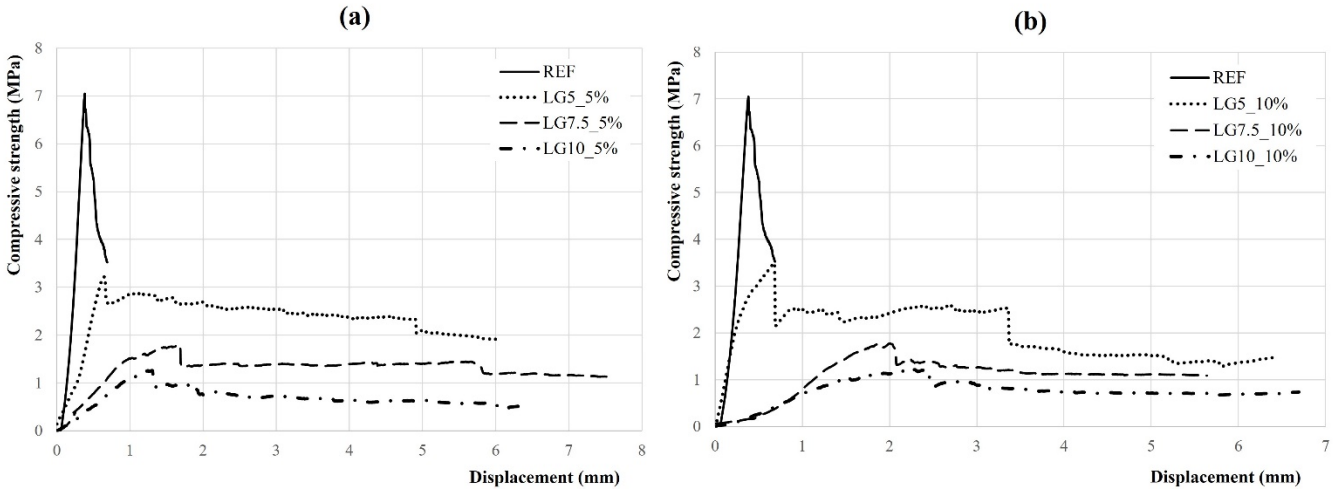

Figure 6 Compressive strengths of LG samples manufactured with foaming agent diluted respectively at 5% (a) and 10% (b).

Figure 7 LG10_5% sample after compressive test.

Table 6 Mechanical properties of the reference and all the lightweight gypsum samples

Sample	Flexural strength, σ_f (MPa)	Compressive strength, σ_c (MPa)
REF	4.19 ± 0.14	6.98 ± 0.12
LG5_5%	2.00 ± 0.13	3.17 ± 0.15
LG7.5_5%	1.40 ± 0.18	1.77 ± 0.10
LG10_5%	1.07 ± 0.19	1.26 ± 0.40
LG5_10%	2.20 ± 0.10	3.43 ± 0.84
LG7.5_10%	1.48 ± 0.11	1.87 ± 0.08
LG10_10%	1.16 ± 0.14	1.45 ± 0.16

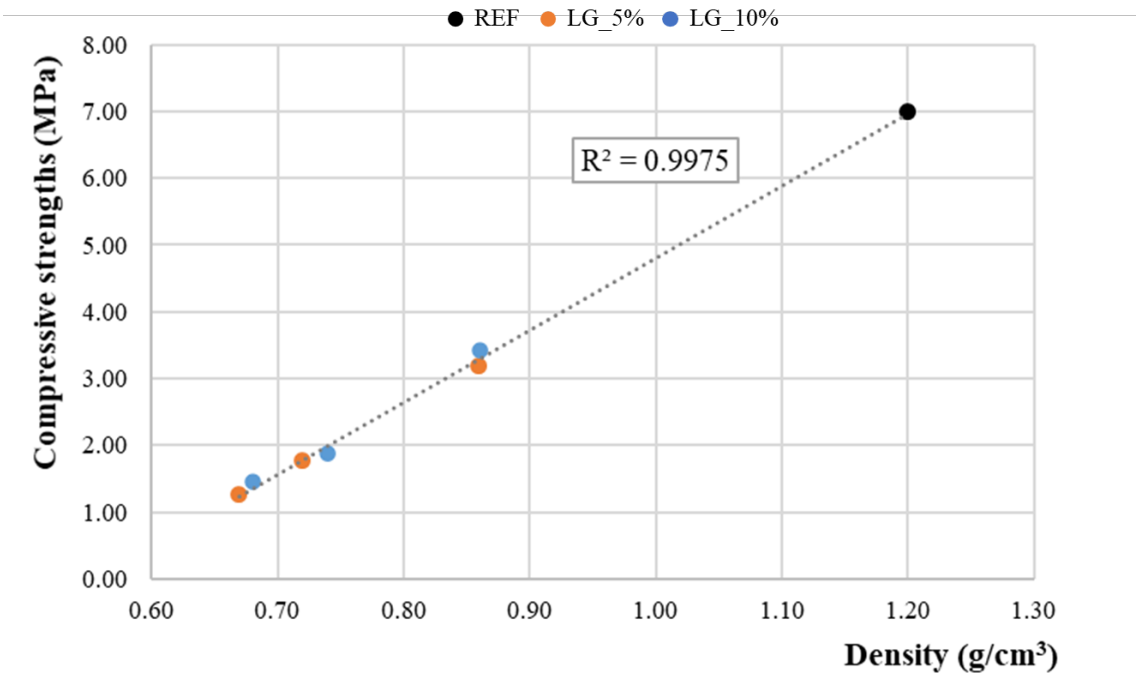

Figure 8 Correlation between bulk density and compressive strength for REF and all LG samples.

The results discussed until now, demonstrated that the different dilution of the FA (i.e. 5% and 10%) did not considerably affect the main physical and mechanical features of the LG samples. So, in the further experimental campaign, only the LG samples obtained with a 5% dilution of foaming agent were investigated.

3.4 X-ray Micro-tomography characterization

A visual inspection of the micro-CT gray-scale images of the four analyzed samples show that they are constituted by a gray matrix (hemihydrate), with dispersed highly-attenuating white grains (calcite and anhydrite) and black (poorly-attenuating) pores, see Fig. 9.

The reconstructed three-dimensional volume rendering for each sample has been used to measure porosity percentage, as well as pores connectivity, size and distribution. In general the porosity includes large spherical bubbles (≥ 10 μm in diameter), produced by the foaming agent and randomly distributed in the sample, and smaller (mostly between 5-10 μm in diameter) gypsum matrix-pores possibly inherited by voids initially present in the gypsum powder, Fig.10.

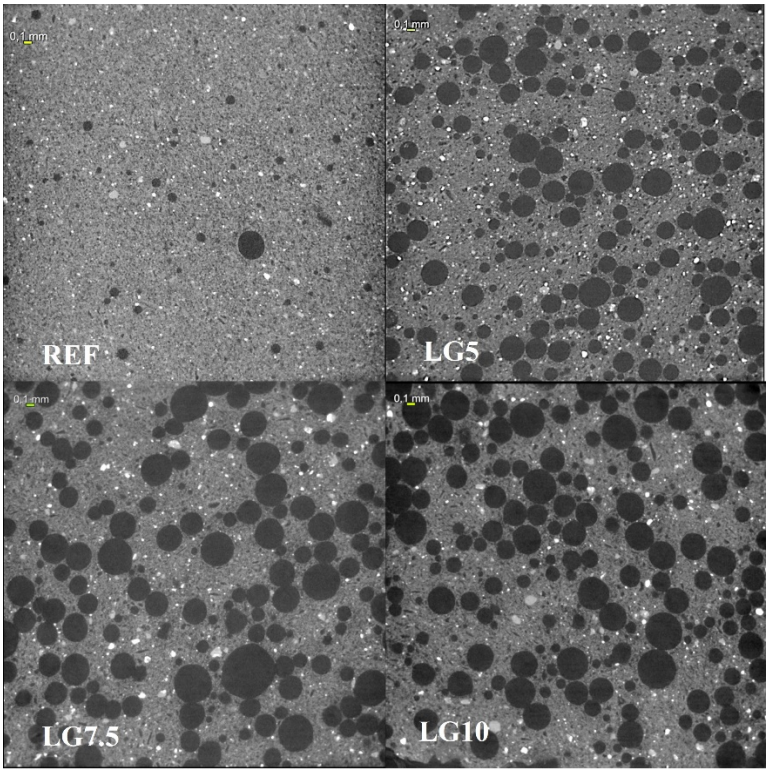

Figure 9 Examples of Micro-CT gray-scale slices of analysed samples: black areas represent low-density pores, white spots are high density grains (calcite and anhydrite). The side of each slice is 5 mm.

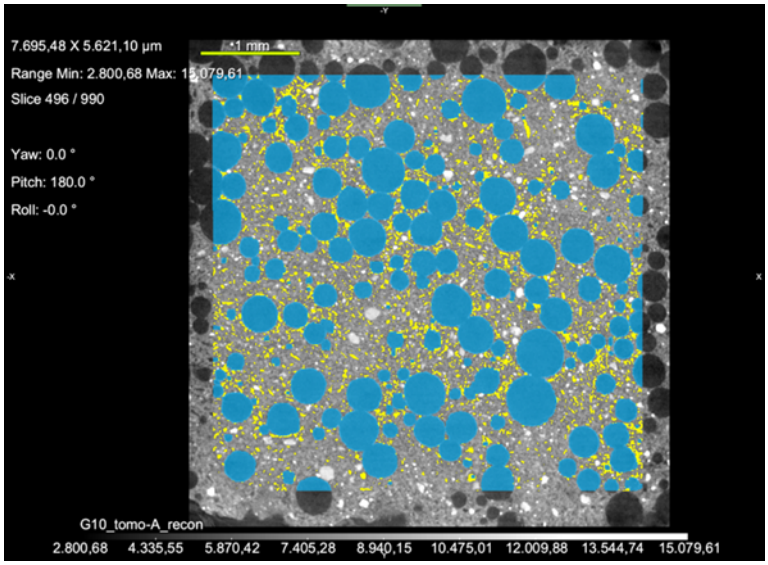

Figure 10 Segmented pores: in blue large bubbles and in yellow gypsum matrix-pores

Micro-CT data, summarized in Table 7, show that total porosity percentage (by volume) increases according to the amounts of foaming agent in the sample, from 48.72% in REF (which is the typical porosity of a gypsum matrix), to 63.58% in LG5_5%, to 67.47% in LG7.5_5%, to 69.62% in LG10_5%. In particular the increment in porosity is mainly due to the growing of the total volume (number and diameter) of the large bubbles in LG samples, while the microstructure of the gypsum matrix-pores remains unchanged in LG samples and similar to that of REF. It is worth noting that the total porosity values obtained by Micro-CT are definitely comparable to those obtained by water absorption test, reported in Table 4. Therefore, it is possible to deduce that all the samples do not exhibit closed porosity.

Table 7 Micro-CT 3D Textural parameters

Sample	Total porosity (% vol)	Gypsum matrix pores (% vol)	Large bubbles (% vol)	Connected porosity (% vol)
REF	48.72	48.72	-	-
LG5_5%	63.58	34.59	28.99	92.06%
LG7.5_5%	67.47	30.89	36.58	95.29%
LG10_5%	69.62	28.85	40.77	96.78%

As the amount of foaming agent in LG samples essentially affects the characteristic of large bubbles (but left unchanged the structure of gypsum matrix-pores), a detailed estimation on their size, distribution, and connectivity was performed, to better define the possible relation between large

pores structure and material properties. The distribution and size of the large bubbles in the analyzed samples are shown in Fig. 11. A slightly increment in the volume of the bubbles (mainly due to coalescence) is observable passing from LG5_5% to LG7.5_5% to LG10_5%.

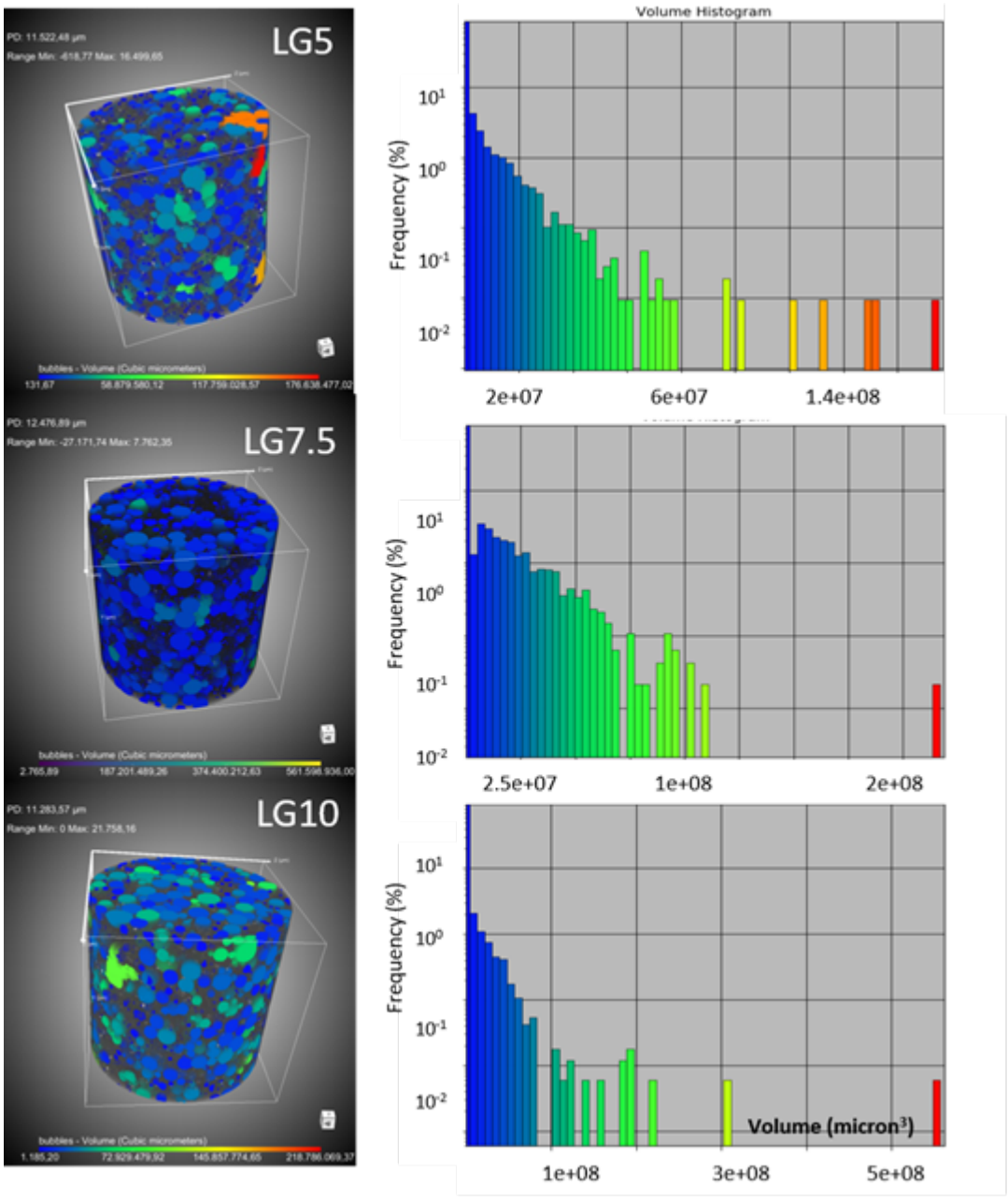

Figure 11 3D distribution and size of large bubbles in LG_5% samples

Moreover, the connectivity between pores is displayed in Fig. 12. In particular the spheres represent the centroid of each connected pore and the size of the spheres is proportional to the number of connected pores. The connectivity is quite similar in the three analyzed samples.

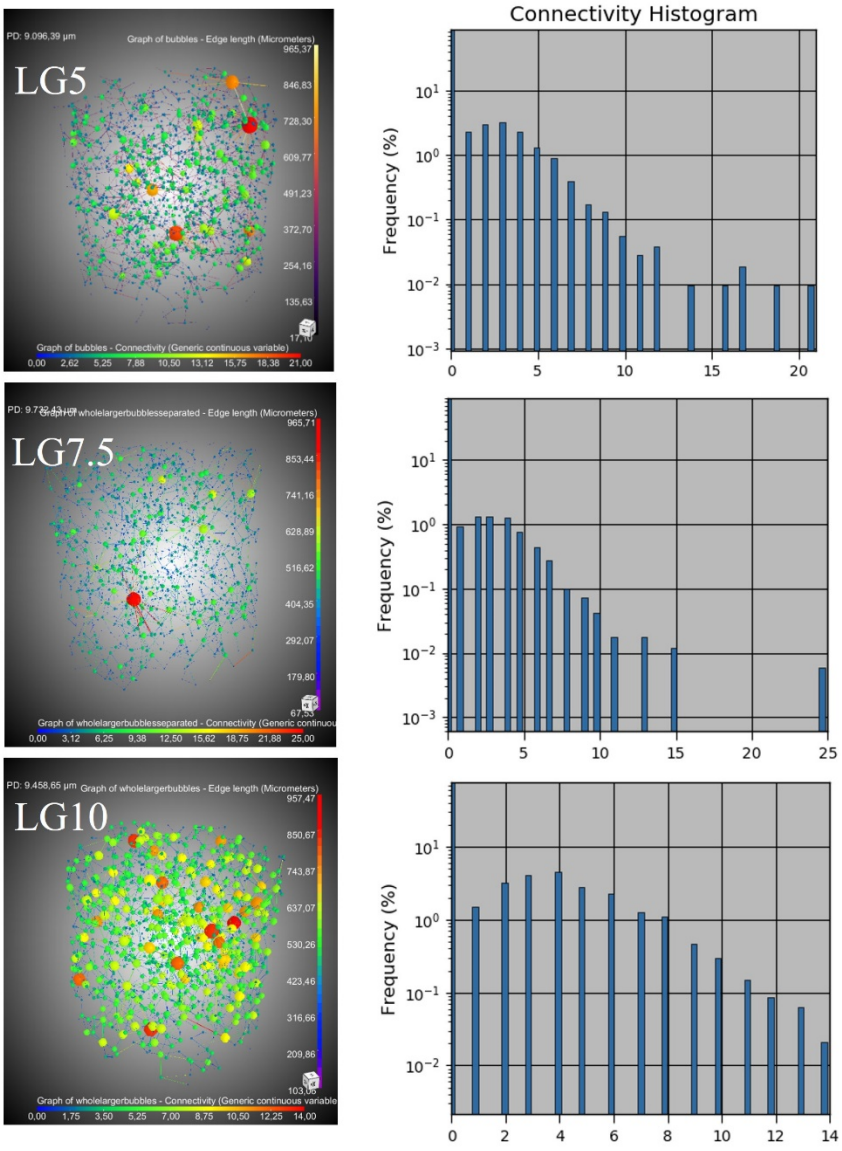

Figure 12 Pores connectivity of LG_5% samples

Summing up, Micro-CT investigations revealed that the microstructure of the analyzed LG samples is characterized by 1) even-distributed fine irregularly-shaped pores, possibly inherited by voids initially present in the gypsum matrix and 2) uneven-distributed large size and connected pores, produced by the foaming agent. In particular, the latter show an high degree of connectivity and porosity volumes that increase with the amount of foaming agent from 28.99% (LG5_5%) to 40.77 (LG10_5%). This transition in porosity value of the large connected bubbles is particularly important as it controls the so-called percolation threshold (ϕc) that corresponds to the minimum value of the connected porosity at which extended connected networks exist. Following standard percolation theory when porosity is slightly greater than ϕc, the permeability increases rapidly with increasing porosity following a power law relationship. Moreover standard percolation theory shows that if uniform spheres are placed randomly in a much larger sample volume and the spheres

are allowed to overlap (connect), then a cluster of touching and overlapping spheres will span the sample volume at ϕ (porosity) = ϕc = 28.5 vol% [48]. For this reason a percolation threshold at $\phi \sim$ 30% is generally assumed [49]. In this view, in our LG samples this threshold is achieved roughly between LG5_5% and LG7.5_5%.

3.5 Thermal and acoustic properties

As above mentioned, the discussion on the thermal insulation and sound-absorbing properties of the insulating behavior will be hereafter limited to the samples manufactured with the 5% dilution of the foaming agent. In particular, thermal conductivities of REF and LG samples are summarized in Table 8, along with the densities previously discussed (see Table 4). The data showed a significant influence of the foaming agent amount on the thermal conductivity, and that these latter appear to be correlated by a direct proportionality (see Fig. 13). Moreover, it is possible to observe that, as expected from literature [50,51], the thermal conductivity decreases for lower densities, as air has lower lambda than solids. In particular, a reduction respect to REF sample of about 39% and 56%, respectively for LG7.5_5% and LG10_5% samples was detected (Table 8). Interestingly, a strong relationship between thermal conductivity with growing and expansion of pores has been recently predicted on the basis of high-speed synchrotron X-ray imaging of glass foaming and thermal conductivity simulation [52]. It is worth noting that the values of thermal conductivity obtained for LG samples resulted to be absolutely comparable with the values exhibited by foamed gypsum composites [23] and inorganic lightweight materials for thermal insulation [51,53]. Furthermore, materials characterized by a not too high thermal insulation and a suitable weight, like LG samples produced, can be used in warmer climatic areas where the achievement of effective building energy saving requires not only low thermal conductivity values, but a proper balance between thermal insulation and thermal capacity.

Table 8 Thermal conductivity (**λ**) of the reference and lightweight gypsum samples obtained with 5% dilution of foaming agent.

Sample	Thermal conductivity, λ (W/m·K)	Density, ρ (g/cm^3)
REF	0.57 ± 0.02	1.20 ± 0.02
LG5_5%	0.46 ± 0.04	0.86 ± 0.05
LG7.5_5%	0.35 ± 0.05	0.72 ± 0.03
LG10_5%	0.25 ± 0.04	0.67 ± 0.09

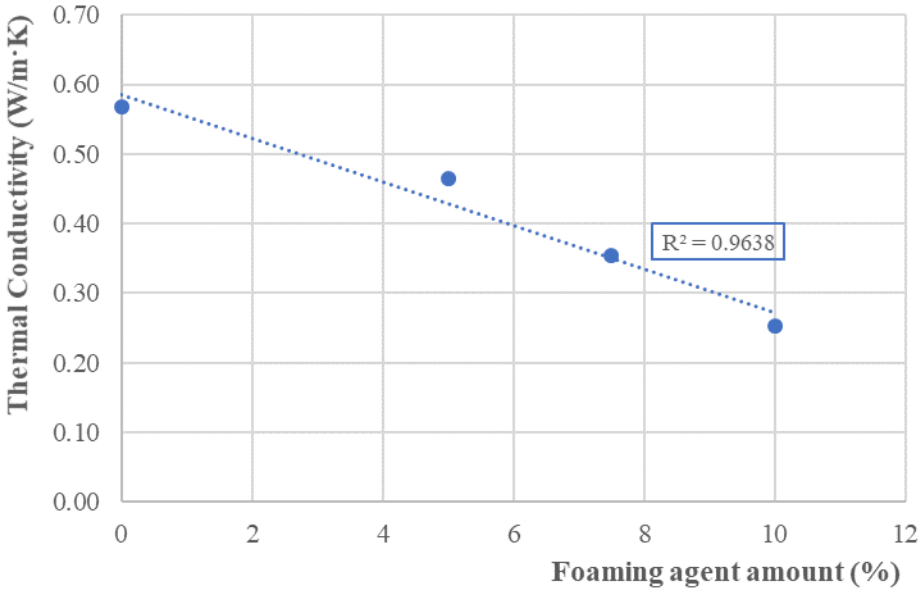

Figure 13 Correlation between thermal conductivity and amount of foaming agent for LG samples obtained with 5% dilution.

The value of the normal incidence sound absorption coefficient α_0 versus frequency obtained as described in section 2.3.4 is reported for the three LG samples and for the reference gypsum in Fig. 14. The acoustic results show that the normal incidence sound absorption coefficient values of LG samples are higher than one of reference gypsum, due to the increase of the total porosity as well as the connected porosity (see Table 7). However, whereas for the LG5_5% sample the improvement of sound-absorbing features is very poor, for the LG7.5_5% and LG10_5% samples it is quite remarkable. In fact, the average value of the normal incidence sound absorption coefficient in the considered frequency range changes from 0.05 for REF sample to 0.07 for LG5_5% sample up to 0.16 and 0.15 for LG7.5_5% and LG10_5% samples respectively. Therefore the acoustic results show that the amount of foaming agent has to be at least 7.5 % to give quite relevant sound-absorbing features to lightweight foamed gypsum samples. This significant increment of sound absorption coefficient for the LG7.5_5% and LG10_5% can be related to the above discussed exceeding of the critical porosity value (about 30%), which corresponds to a substantial permeability growth. Moreover, the slightly lower value of the normal incidence sound absorption coefficient for LG10_5% sample with respect to LG7.5_5% sample is probably due the higher tortuosity value for the former than the latter. However, this issue needs to be further investigated.

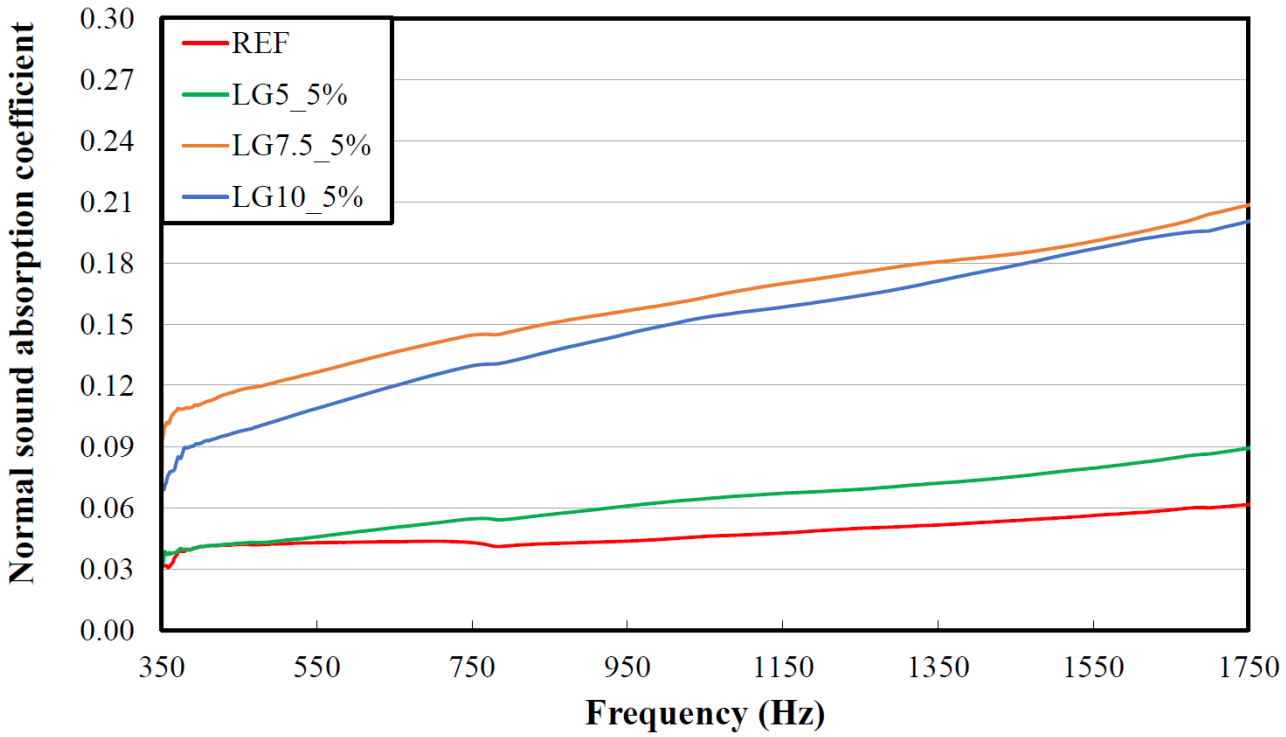

Figure 14 Normal sound absorption coefficient (α_0) of the REF and LG samples.

4. Conclusions

In the present paper, a foaming agent, made mainly of natural surfactants dissolved in water solution, has been used to produce lightweight gypsum composites. In particular, two foaming agent formulations, based on 5% and 10% dilutions (wt/wt) of the pure foaming agent solution, were selected and their foaming properties were preliminarily investigated. Then, different amounts (5, 7.5 and 10% wt) of pre-manufactured foams obtained from the whipping of the foaming agent solutions, were added to the gypsum matrices in order to lighten them. The effects of the porosity increase induced by the foaming agent addition, on the physical, mechanical and morphological features of the gypsum composites were widely evaluated. Also the enhancement of the thermal insulating and sound-absorbing properties of the lightweight gypsum was investigated. The use of surfactant-based foaming agent, led to a reduction of the setting time of fresh gypsum pastes, even if this effect tends to lower with the increase of foaming agent amount. The experimental results demonstrated that, while the different dilutions of the foaming agent did not affect significantly neither the main physical properties nor the mechanical behaviour of the LG samples, the addition of higher amounts of foaming agent influenced considerably both of them. In fact, the increase of foaming agent content caused a reduction of flexural strength and a modification of the compressive behavior, due to a toughening effect related to the porosity increase. Also thermal conductivity

resulted to be influenced by the percentage of foaming agent, in particular the conductivity values decreased proportionally with the increase of foaming agent addition. Finally the acoustic behavior of the gypsum foams revealed that the increase of the total porosity as well as the connected one, translated into higher values of normal incidence sound absorption coefficient compared to REF sample. Moreover, micro-CT analyses confirmed that the porosity percentage in gypsum matrices increased for higher amounts of foaming agent and that the large pores obtained are strongly interconnected. Particularly the Micro-CT results show that microstructure of analyzed LG samples includes both small gypsum matrix pores possibly inherited by voids initially present in the gypsum powder as well as large pores whose total porosity (number and diameter) increases according with the amount of foaming agent. This porosity variation of the large bubble population influences permeability behavior (percolation threshold) and thus material proprieties. A significant variation in both thermal conductivity as well as acoustic proprieties has been observed when a critical porosity threshold is reached between LG5_5% (under the threshold) and LG7.5_5% -LG10_5% samples (both above the threshold).

It is possible to conclude that the lightweight gypsum-based composites studied in the present investigation, can be successfully proposed as innovative and sustainable building materials for thermal insulation and sound absorbing applications.

Conflict of Interest: The authors declare that they have no conflict of interest.

References

[1] N. Değirmenci, Utilization of phosphogypsum as raw and calcined material in manufacturing of building products, Constr. Build. Mater. 22 (2008) 1857–1862. https://doi.org/10.1016/j.conbuildmat.2007.04.024.

[2] P. Tesárek, J. Drchalová, J. Kolísko, P. Rovnaníková, R. Černý, Flue gas desulfurization gypsum: Study of basic mechanical, hydric and thermal properties, Constr. Build. Mater. 21 (2007) 1500–1509. https://doi.org/10.1016/j.conbuildmat.2006.05.009.

[3] M. Doleželová, J. Krejsová, A. Vimmrová, Lightweight gypsum based materials: Methods of preparation and utilization, Int. J. Sustain. Dev. Plan. 12 (2017) 326–335. https://doi.org/10.2495/SDP-V12-N2-326-335.

[4] O. Gencel, J.J. Del Coz Diaz, M. Sutcu, F. Koksal, F.P. Álvarez Rabanal, G. Martínez-

Barrera, A novel lightweight gypsum composite with diatomite and polypropylene fibers, Constr. Build. Mater. 113 (2016) 732–740. https://doi.org/10.1016/j.conbuildmat.2016.03.125.

[5] C. Martias, Y. Joliff, C. Favotto, Effects of the addition of glass fibers, mica and vermiculite on the mechanical properties of a gypsum-based composite at room temperature and during a fire test, Compos. Part B Eng. 62 (2014) 37–53. https://doi.org/10.1016/j.compositesb.2014.02.019.

[6] J. Jiang, Z. Lu, J. Li, Y. Fan, Y. Niu, Preparation and hardened properties of lightweight gypsum plaster based on pre-swelled bentonite, Constr. Build. Mater. 215 (2019) 360–370. https://doi.org/10.1016/j.conbuildmat.2019.04.181.

[7] A. Vimmrová, M. Keppert, L. Svoboda, R. Černý, Lightweight gypsum composites: Design strategies for multi-functionality, Cem. Concr. Compos. 33 (2011) 84–89. https://doi.org/10.1016/j.cemconcomp.2010.09.011.

[8] F. Iucolano, B. Liguori, P. Aprea, D. Caputo, Thermo-mechanical behaviour of hemp fibers-reinforced gypsum plasters, Constr. Build. Mater. 185 (2018) 256–263. https://doi.org/10.1016/j.conbuildmat.2018.07.036.

[9] F. Iucolano, L. Boccarusso, A. Langella, Hemp as eco-friendly substitute of glass fibres for gypsum reinforcement: Impact and flexural behaviour, Compos. Part B Eng. 175 (2019). https://doi.org/10.1016/j.compositesb.2019.107073.

[10] S. Gutiérrez-González, J. Gadea, A. Rodríguez, C. Junco, V. Calderón, Lightweight plaster materials with enhanced thermal properties made with polyurethane foam wastes, Constr. Build. Mater. 28 (2012) 653–658. https://doi.org/10.1016/j.conbuildmat.2011.10.055.

[11] C. Dima, A. Badanoiu, S. Cirstea, A.I. Nicoara, S. Stoleriu, Lightweight gypsum materials with potential use for thermal insulations, Materials (Basel). 13 (2020) 1–13. https://doi.org/10.3390/ma13235454.

[12] I. Capasso, F. Iucolano, Production of lightweight gypsum using a vegetal protein as foaming agent, Mater. Struct. Constr. 53 (2020) 1–13. https://doi.org/10.1617/s11527-020-01469-w.

[13] R.K. Nishihora, P.L. Rachadel, M.G.N. Quadri, D. Hotza, Manufacturing porous ceramic materials by tape casting—A review, J. Eur. Ceram. Soc. 38 (2018) 988–1001. https://doi.org/10.1016/J.JEURCERAMSOC.2017.11.047.

[14] F.N. Arroyo, A.L. Christoforo, V.R. Salvini, P.I.B.G.B. Pelissari, V.C. Pandolfelli, A.P. Luz, C.A. Cardoso, Development of plaster foam for thermal and acoustic applications, Constr. Build. Mater. 262 (2020) 120800. https://doi.org/10.1016/j.conbuildmat.2020.120800.

[15] B. Liguori, F. Iucolano, I. Capasso, M. Lavorgna, L. Verdolotti, The effect of recycled plastic aggregate on chemico-physical and functional properties of composite mortars, Mater. Des. 57 (2014) 578–584. https://doi.org/10.1016/j.matdes.2014.01.006.

[16] J. König, A. Lopez-Gil, P. Cimavilla-Roman, M.A. Rodriguez-Perez, R.R. Petersen, M.B. Østergaard, N. Iversen, Y. Yue, M. Spreitzer, Synthesis and properties of open- and closed-porous foamed glass with a low density, Constr. Build. Mater. 247 (2020) 118574. https://doi.org/10.1016/J.CONBUILDMAT.2020.118574.

[17] I.S. Vicario, L.A. Cuenca-Romero, S.G. González, V.C. Carpintero, Á.R. Saiz, Design and Characterization of Gypsum Mortars Dosed with Polyurethane Foam Waste PFW, Mater. 2020, Vol. 13, Page 1497. 13 (2020) 1497. https://doi.org/10.3390/MA13071497.

[18] P. Umponpanarat, S. Wansom, Thermal conductivity and strength of foamed gypsum formulated using aluminum sulfate and sodium bicarbonate as gas-producing additives, Mater. Struct. Constr. 49 (2016) 1115–1126. https://doi.org/10.1617/s11527-015-0562-1.

[19] B. Galzerano, I. Capasso, L. Verdolotti, M. Lavorgna, P. Vollaro, D. Caputo, S. Iannace, B. Liguori, Design of sustainable porous materials based on 3D-structured silica exoskeletons, Diatomite: Chemico-physical and functional properties, Mater. Des. 145 (2018) 196–204. https://doi.org/10.1016/j.matdes.2018.02.063.

[20] I. Capasso, B. Liguori, L. Verdolotti, D. Caputo, M. Lavorgna, E. Tervoort, Process strategy to fabricate a hierarchical porosity gradient in diatomite-based foams by 3D printing, Sci. Rep. 10 (2020). https://doi.org/10.1038/s41598-019-55582-0.

[21] A. Colak, Density and strength characteristics of foamed gypsum, Cem. Concr. Compos. 22 (2000). http://www.sciencedirect.com/science/article/pii/S0958946500000081.

[22] O. Gencel, J.J. Del Coz Diaz, M. Sutcu, F. Koksal, F.P. Alvarez Rabanal, G. Martinez-Barrera, W. Brostow, Properties of gypsum composites containing vermiculite and polypropylene fibers: Numerical and experimental results, Energy Build. 70 (2014) 135–144. https://doi.org/10.1016/j.enbuild.2013.11.047.

[23] J.C. Rubio-Avalos, A. Manzano-Ramírez, J.M. Yañez-Limón, M.E. Contreras-García, E.M. Alonso-Guzmán, J. González-Hernández, Development and characterization of an inorganic

foam obtained by using sodium bicarbonate as a gas generator, Constr. Build. Mater. 19 (2005) 543–549. https://doi.org/10.1016/j.conbuildmat.2004.12.001.

[24] Z. Bazelová, L. Pach, J. Lokaj, The effect of surface active substance concentration on the properties of foamed and non-foamed gypsum, Ceram. - Silikaty. 54 (2010) 379–385.

[25] A. Just, B. Middendorf, Microstructure of high-strength foam concrete, Mater. Charact. 60 (2009) 741–748. https://doi.org/10.1016/j.matchar.2008.12.011.

[26] L. Verdolotti, B. Liguori, I. Capasso, A. Errico, D. Caputo, M. Lavorgna, S. Iannace, Synergistic effect of vegetable protein and silicon addition on geopolymeric foams properties, J. Mater. Sci. 50 (2014) 2459–2466. https://doi.org/10.1007/s10853-014-8801-3.

[27] B. Galzerano, L. Verdolotti, I. Capasso, B. Liguori, Setting up the production process of diatomite-based ceramic foams, Mater. Manuf. Process. 33 (2018) 1648–1653. https://doi.org/10.1080/10426914.2017.1415449.

[28] M. Hammershøj, A. Prins, K.B. Qvist, Influence of pH on surface properties of aqueous egg albumen solutions in relation to foaming behaviour, J. Sci. Food Agric. 79 (1999) 859–868. https://doi.org/10.1002/(SICI)1097-0010(19990501)79:6<859::AID-JSFA301>3.0.CO;2-C.

[29] M. Hammershøj, K.B. Qvist, Research Note: Importance of Hen Age and Egg Storage Time for Egg Albumen Foaming, LWT - Food Sci. Technol. 34 (2001) 118–120. https://doi.org/10.1006/fstl.2000.0750.

[30] UNI EN 196-3. Methods of testing cement – Part 3: determination of setting times and soundness, (2009).

[31] UNI 11060:2003 - Beni culturali - Materiali lapidei naturali ed artificiali - Determinazione della massa volumica e della percentuale di vuoti, (2003). http://store.uni.com/catalogo/uni-11060-2003?josso_back_to=http://store.uni.com/josso-security-check.php&josso_cmd=login_optional&josso_partnerapp_host=store.uni.com.

[32] UNI EN 14579-2005 Natural stone test methods - Determination of sound speed propagation., (2005).

[33] Y. Akkaya, T. Voigt, K. V. Subramaniam, S.P. Shah, Nondestructive measurement of concrete strength gain by an ultrasonic wave reflection method, Mater. Struct. 36 (2003) 507–514. https://doi.org/10.1007/bf02480827.

[34] B. Ercikdi, T. Yilmaz, G. Külekci, Strength and ultrasonic properties of cemented paste

backfill, Ultrasonics. 54 (2014) 195–204. https://doi.org/10.1016/j.ultras.2013.04.013.

[35] I.L. Meglis, T. Chow, C.D. Martin, R.P. Young, Assessing in situ microcrack damage using ultrasonic velocity tomography, Int. J. Rock Mech. Min. Sci. 42 (2005) 25–34. https://doi.org/10.1016/j.ijrmms.2004.06.002.

[36] UNI EN 1015-11. Methods of test for mortar for masonry – Part 11: determination of flexural and compressive strength of hardened mortar., (2007).

[37] L. Pappalardo, G. Buono, S. Fanara, P. Petrosino, Combining textural and geochemical investigations to explore the dynamics of magma ascent during Plinian eruptions: a Somma–Vesuvius volcano (Italy) case study, Contrib. to Mineral. Petrol. 173 (2018) 61. https://doi.org/10.1007/s00410-018-1486-x.

[38] A. Liedl, G. Buono, G. Lanzafame, S.D.- Lithos, undefined 2019, A 3D imaging textural characterization of pyroclastic products from the 1538 AD Monte Nuovo eruption (Campi Flegrei, Italy), Elsevier. (n.d.). https://www.sciencedirect.com/science/article/pii/S002449371930194X (accessed June 21, 2021).

[39] ASTM WK43689 - New Test Method for Thermal Effusivity Using a Modified Transient Plane Source Method, 2015., (2015).

[40] ASTM WK50791 - New Test Method for Thermal Effusivity Calibration of the Modified Transient Plane Source Apparatus., (2013).

[41] J.Y. Chung, D.A. Blaser, Transfer function method of measuring in-duct acoustic properties. I. Theory, J. Acoust. Soc. Am. 68 (1980) 907–913. https://doi.org/10.1121/1.384778.

[42] EN ISO 10534-2. Acoustic - Determination of sound absorption coefficient and impedance in impedances tubes - Part 2: Transfer-function method., (2001).

[43] J.Y. Chung, A. Blaser, Transfer function method of measuring in-duct acoustic properties. II. Experiment, J. Acoust. Soc. Am. 68 (1980) 914–921. https://doi.org/10.1121/1.384779.

[44] H. Böke, S. Akkurt, S. Özdemir, E.H. Göktürk, E.N. Caner Saltik, Quantification of CaCO3–CaSO3·0.5H2O–CaSO4·2H2O mixtures by FTIR analysis and its ANN model, Mater. Lett. 58 (2004) 723–726. https://doi.org/10.1016/J.MATLET.2003.07.008.

[45] M. Francesco, L. Russa, S.A. Ruffolo, G. Barone, G.M. Crisci, P. Mazzoleni, A. Pezzino, The Use of FTIR and Micro-FTIR Spectroscopy: An Example of Application to Cultural

Heritage, Int. J. Spectrosc. 893528 (2009). https://doi.org/10.1155/2009/893528.

[46] F. Iucolano, B. Liguori, D. Caputo, F. Colangelo, R. Cioffi, Recycled plastic aggregate in mortars composition: Effect on physical and mechanical properties, Mater. Des. 52 (2013) 916–922. https://doi.org/10.1016/j.matdes.2013.06.025.

[47] L. Montanaro, Y. Jorand, G. Fantozzi, A. Negro, Ceramic foams by powder processing, J. Eur. Ceram. Soc. 18 (2002) 1339–1350. https://doi.org/10.1016/s0955-2219(98)00063-6.

[48] M. Sahini, M. Sahimi, Applications Of Percolation Theory, CRC Press, London, 1994. https://doi.org/10.1201/9781482272444.

[49] E.J. Garboczi, K.A. Snyder, J.F. Douglas, M.F. Thorpe, Geometrical percolation threshold of overlapping ellipsoids, Phys. Rev. E. 52 (1995) 819–828. https://doi.org/10.1103/PhysRevE.52.819.

[50] I. Asadi, P. Shafigh, Z.F. Bin Abu Hassan, N.B. Mahyuddin, Thermal conductivity of concrete – A review, J. Build. Eng. 20 (2018) 81–93. https://doi.org/10.1016/j.jobe.2018.07.002.

[51] L. Verdolotti, F. Iucolano, I. Capasso, M. Lavorgna, S. Iannace, B. Liguori, Recycling and recovery of PE-PP-PET-based fiber polymeric wastes as aggregate replacement in lightweight mortar: Evaluation of environmental friendly application, Environ. Prog. Sustain. Energy. 33 (2014) 1445–1451. https://doi.org/10.1002/ep.11921.

[52] M.B. Østergaard, M. Zhang, X. Shen, R.R. Petersen, J. König, P.D. Lee, Y. Yue, B. Cai, High-speed synchrotron X-ray imaging of glass foaming and thermal conductivity simulation, Acta Mater. 189 (2020) 85–92. https://doi.org/10.1016/j.actamat.2020.02.060.

[53] S.F.A. Zaidi, E. Ul Haq, K. Nur, N. Ejaz, M. Anis-ur-Rehman, M. Zubair, M. Naveed, Synthesis & characterization of natural soil based inorganic polymer foam for thermal insulations, Constr. Build. Mater. 157 (2017) 994–1000. https://doi.org/10.1016/j.conbuildmat.2017.09.112.